frontiers | Frontiers in Marine Science

TYPE Original Research
PUBLISHED 26 July 2022
DOI 10.3389/fmars.2022.937616

OPEN ACCESS

EDITED BY
Joseph Carlin,
California State University, Fullerton, United States

REVIEWED BY
Jiantao Cao,
Tongji University, China
Qiang Xie,
Chinese Academy of Sciences (CAS), China

*CORRESPONDENCE
Gang Li
gangli@scsio.ac.cn

SPECIALTY SECTION
This article was submitted to Coastal Ocean Processes, a section of the journal Frontiers in Marine Science

RECEIVED 06 May 2022
ACCEPTED 29 June 2022
PUBLISHED 26 July 2022

CITATION
Li G, Miao L and Yan W (2022) Holocene evolution of the shelf mud deposits in the north-western South China Sea. *Front. Mar. Sci.* 9:937616. doi: 10.3389/fmars.2022.937616

Holocene evolution of the shelf mud deposits in the north-western South China Sea

Gang Li[1,2]*, Li Miao[1,2] and Wen Yan[3]

[1]Southern Marine Science and Engineering Guangdong Laboratory (Guangzhou), Guangzhou, China, [2]Key Laboratory of Ocean and Marginal Sea Geology, South China Sea Institute of Oceanology, Innovation Academy of South China Sea Ecology and Environmental Engineering, Chinese Academy of Sciences, Guangzhou, China, [3]University of Chinese Academy of Sciences, Beijing, China

Marine mud deposits contain rich information on past interactions between riverine sediment fluxes and marine processes. Massive mud deposits attached to a major river from South China, the Pearl River, are distributed on the north-western shelf of the South China Sea. This study examines the evolution history using cores penetrating through Holocene strata and deciphers its response to the river system, sea-level change, monsoon variations, human activities, etc. Geochemical and sedimentological data constrained by robust radiocarbon data show the difference in the evolution of mud deposits in shallow waters and on the middle shelf. Muddy wedges in shallow waters along the coast have formed since 7 ka BP, when modern current systems were established during the middle Holocene sea-level highstand. However, wide-spread muddy deposits in the middle shelf initiated after 3 ka BP which are associated with enhanced sediment fluxes and strengthened winter monsoon. Human activities on recent millennia have play a significant role in influencing the mud deposition on the north-west shelf of the South China Sea, as evidenced by the enrichment of heavy metals in marine sediments.

KEYWORDS

shelf muddy sediments, sea-level changes, Pearl River, northern South China Sea, human activity

Introduction

Mud deposits are widely distributed on the continental shelf of the world and are an important archive of past environmental changes (Nizou et al., 2010; Bassetti et al., 2016). Mud successions on the shelf provide very high-resolution records of oceanic circulations and climate changes (Wang et al., 2014). However, sedimentary records of shelf deposits

are rarely continuous over a long period because the formation is influenced by complex interactions such as sea-level conditions, sediment supply, transport and accumulation processes, and shelf morphology (see the thorough reviews by Gao and Collins, 2014; Hanebuth et al., 2015). To fully understand these sedimentary records, it is necessary to obtain knowledge about the process–product relationships of mud deposits on the shelf.

As coastal rivers in China carry enormous amounts of sediment into the continental margin, this massive sedimentation is responsible for the occurrence of the widest continental shelves on earth (Wang, 1999). Most of the fine-grained sediments from rivers are trapped on the wide shelf and build various mud deposits in different water depths. Two types of muddy depositional systems were identified, i.e., isolated eddy muddy bodies on the shelf and coast-attached muddy zones (Gao and Collins, 2014; Li et al., 2014). Isolated eddy mud deposits are generally present in calm hydrodynamic environments on the middle and outer shelf and are associated with shelf currents favorable for fine-grained sediment transport and deposition (Li et al., 2014). Mud deposits found on the middle and outer shelf were mostly formed during the transgression period (Park et al., 2000). Coastal mud deposits on the inner shelf are mostly attached to big rivers, such as the Shandong Peninsula muddy belt in the northern Yellow Sea (Liu et al., 2009) and the Zhe-Min mud belt in the East China Sea (Liu et al., 2007). As the distal sink of river-discharged suspended sediments, the formation and evolution of coastal mud deposits is closely correlated with the evolution of river systems (Liu et al., 2007; Gao and Collins, 2014; Gao et al., 2015; Xu et al., 2012). The sea-level change also plays a significant role on the formation of coastal mud deposits and most initiated after the attainment of the high sea-level stand (Liu et al., 2007; Li et al., 2014). Provenance studies on coastal mud deposits in the East China Sea revealed the role of coastal currents associated with the East Asian monsoon (Chen et al., 2017). Intensive human activities were also proposed to be a potential cause of the increased sedimentation rates of coastal mud wedges during the late Holocene (Xu et al., 2012).

In the north-western South China Sea (SCS), an extensive mud belt attached to the Pear River estuary has an area of more than 8,000 km^2 on the continental shelf (Figure 1A). Liu et al. (2009) and Ge et al. (2014) compiled an isopach map of the Holocene strata on the inner shelf using high-resolution Chirp acoustic profiles. Huang et al. (2018) dated the thick coastal mud wedge in the north-west SCS. However, grain-size analyses on multiple short cores by Liu et al. (2014) and Gao et al. (2015) showed that most mud deposits on the north-west SCS shelf had a thickness of less than 1 m. However, cores penetrating the whole Holocene sequence have not been reported on the north-western SCS shelf. The developmental history of mud depositional systems on this continental shelf has not been well studied.

This study addresses an issue about the developmental history of mud deposits on the northwest SCS shelf by combining previous core records and one new core penetrating Holocene strata. Based on new geochemical and sedimentological data sets, the purpose of this study is to 1) reveal the developmental history of the shelf mud depositional system in the north-western SCS; 2) decipher the formation of shelf mud and its response to the riverine sediment supply, sea-level change, and human activities using robust age constraints.

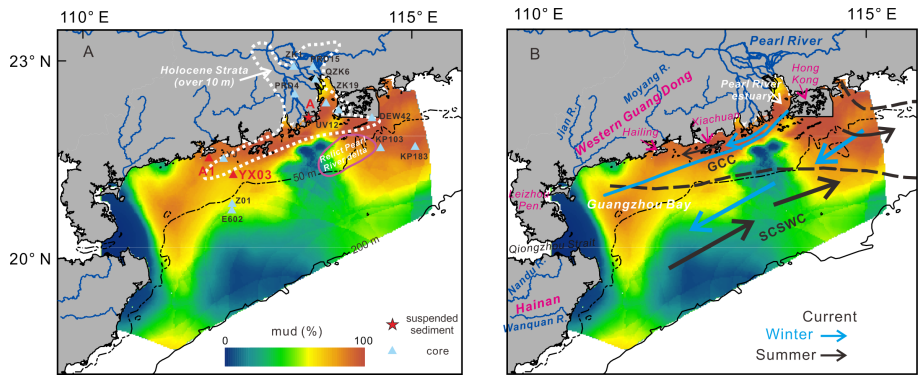

FIGURE 1
The study area and core sites: **(A)** location of new cores (red triangle) and some reference cores (blue triangle) in this study. Grain size data of suspended sediments from the Pearl River was measured by Zheng et al. (2017) at the station **(A)** Dotted lines circle the zones with thick Holocene deposits (>10 m) according to Ge et al. (2014). The relict delta of the Pearl River was mapped by Bao (1995). **(B)** Current systems and freshwater plumes in summer and winter on the northern shelf of South China Sea according to Ding et al. (2017) and Su (2004). GCC, Guangdong coastal current; SCSWC, South China Sea warm current.

Marine settings

The northern continental shelf of the South China Sea has a width of around 200 km and the study area is located from the Pearl River estuary to the east of Hainan Island (Figure 1A). Fluvial sediments are supplied by the Pearl River and other small rivers in the western Guangdong Province and from Hainan Island. The Pearl River annually carries about 80 million tons of suspended sediments to the sea before extensive dam construction (Wang, 1985). The combined sediment fluxes by small rivers are about 3 million tons, including the Moyang River, Jian River and Nandu River (Wang, 2007).

The northern SCS shelf is influenced by the East Asian Monsoon. The north-easterly winds prevail in the winter while the south-westerly winds dominate during the summer. Seasonally reversing monsoon winds play a dominant role in controlling oceanic circulation (Hu et al., 2000; Su, 2004). The Guangdong coastal current (GCC) mainly flows westward in winter and is forced by the north-eastly winds. In summer, the GCC still flows westward along the coast in the north-western SCS, which is driven by fresh-water buoyancy from the Pearl River plume (Bao et al., 2005; Ding et al., 2017) (Figure 1B). On the outer shelf, a stable warm current, i.e., the South China Sea warm current (SCSWC), flows north-eastward along the shelf break during the winter but it spreads over most parts of the continental shelf during the summer (Su, 2004) (Figure 1B).

The highest sediment flux from rivers occurs in summer, taking the form of a suspended sediment plume. Most fine-grained particles from the Pearl River settle out of suspension within the estuary where seawater mixes with freshwater (Wang, 1985). Suspended sediments escaping from the Pearl River estuary are mainly transported alongshore towards the west by the GCC (Wang, 2007). Because the west GCC has a relatively stable speed of over 10 cms^{-1}, fine-grained suspended sediments from the Pearl River can be transported alongshore over a long distance before settling down to the seabed (Gao et al., 2015).

In summer, southerly to south-westerly waves have an average height of 0.5–2.5 m in this study area. In the winter, north-easterly waves have an average height of 0.5–4.0 m. High waves are mainly produced by typhoons, which occur during summer and autumn and have a maximum height of over 10 m (Wang, 2007). Typhoon waves in this study area can cause the re-suspension of sea-bottom sediments on the shelf, even on the outer shelf (Xiao et al., 2013; Zhou, 2014).

Materials and methods

Seabed coring

One gravity core (A1) with a length of 1.74 m was retrieved in 2008 on the coastal mud wedge, south of Hailing Island (111.9°E, 21.55°N; 16 m water depth). One core (YX03) was obtained in 2013 at a water depth of 35.4 m in muddy zones on the middle shelf (112.27°E, 21.29°N). The total length is 29.6 m, and the upper 2.75 m is the Holocene sediments studied in this paper.

Geochemical measurements

To capture the variability of elemental composition of the core YX03, high-resolution XRF measurements (at a 0.5-cm interval) for Al, K, Ti, Ca, Sr, and Fe were performed on core halves at the South China Sea Institute of Oceanology *via* the Geotek Multi-Sensor Core Logger (MSCL). The core surfaces were first flattened and covered with a thin (4 μm) ultralene film to avoid contamination of the prism. Two modes of 10 kV with no filter and 40 kV with a silver filter were used for the analysis with a rhodium X-ray tube. The sample was flushed with helium to prevent partial or complete absorption of the emitted soft radiation from the samples by air. A count time of 30 s was set for each mode. To avoid an overprint of the background signal and the influence of pore-water in core sediments, the element-element ratios or the ratios of a single element against the sum of all element intensities (expressed as "element/sum") are used. Data from some segments with uneven surfaces was excluded.

For further measurements of the core YX03, discrete samples for geochemical and grain-size analyses were taken at the intervals of 10 cm and 1 cm, respectively. The gravity core of A1 was sub-sampled at an interval of 5 cm. For geochemical analyses, approximately 2-gram sediments were dried in a 45°C oven and crushed into powder. Major and trace elements are determined using ICP-OES (Agilent 720) and ICP-MS (Bruker Aurora M90) at the Institute of Geochemistry, following the measurement method by Qi et al. (2000). Data quality was guaranteed using one andesite standard (AMH-1) and one slate standard (OU-6) with a relative error of less than 5%.

Grain-size analysis

To analyze the grain size of terrigenous fractions, biogenic compounds are removed. Samples were treated with a 10% hydrogen peroxide solution under a heated water bath at 60 °C for 12 h to remove organic matters, and acidified with a 20% acetic acid solution at room temperature for 24 h to remove biogenic carbonates. The measurement was performed using a Mastersizer 2000 laser diffraction analyzer.

End-member modeling of grain-size data

Numerical unmixing of grain size distribution data into constituent components, known as end-member analysis

(EMA), can yield valuable information on sediment transport processes, sedimentary environments, and sediment origin (Prins et al., 2000; Tjallingii et al., 2008). To correlate the core records to modern sedimentary environments and identify potential sources, we decomposed all grain-size data in this study using a newly developed GUI software called AnalySize (Paterson and Heslop, 2015; Figure 2).

Chronology

The Holocene stratigraphy of cores YX03 and A1 was constrained by nine ^{14}C-accelerator mass-spectrometric (^{14}C-AMS) dates (Table 1), which were measured on mixed foraminifers and bivalve mollusks. All ^{14}C-AMS dates are calibrated to the calendar year before present using the calibration program Calib 7.0.4 (Reimer et al., 2013), and the additional regional reservoir age of −128 ± 40 is corrected for dates on marine biogenic carbonate shells (Southon et al., 2002).

Results

Lithology and stratigraphy

The Holocene sediments in core YX03 are 2.75 m thick and overlie an erosional surface separating from the Pleistocene mud with a grayish green. The δ^{13}C values of organic carbon in the Pleistocene mud range between −25‰ and −27‰, suggesting it might have been deposited in a lacustrine environment. In the lower section (Section I: 60–275 cm), most sediments are dark gray silty sand with abundant shell fragments, and the mud content is higher in the middle part (145–195 cm). Sediments in section II above 60 cm are brown silt, with very poor sorting and high water content. Shell debris and foraminifera could be seen in the upper 60 cm of core YX03. The core of A1 in offshore waters, south of Hailing Island, mainly consists of yellowish brown silt with variable sand content. In the lower section (50–174 cm), sand is mostly higher than 15%. In section II above 50 cm, sediments are silt-dominated. Compared with the YX03, shell fragments are rare in core A1.

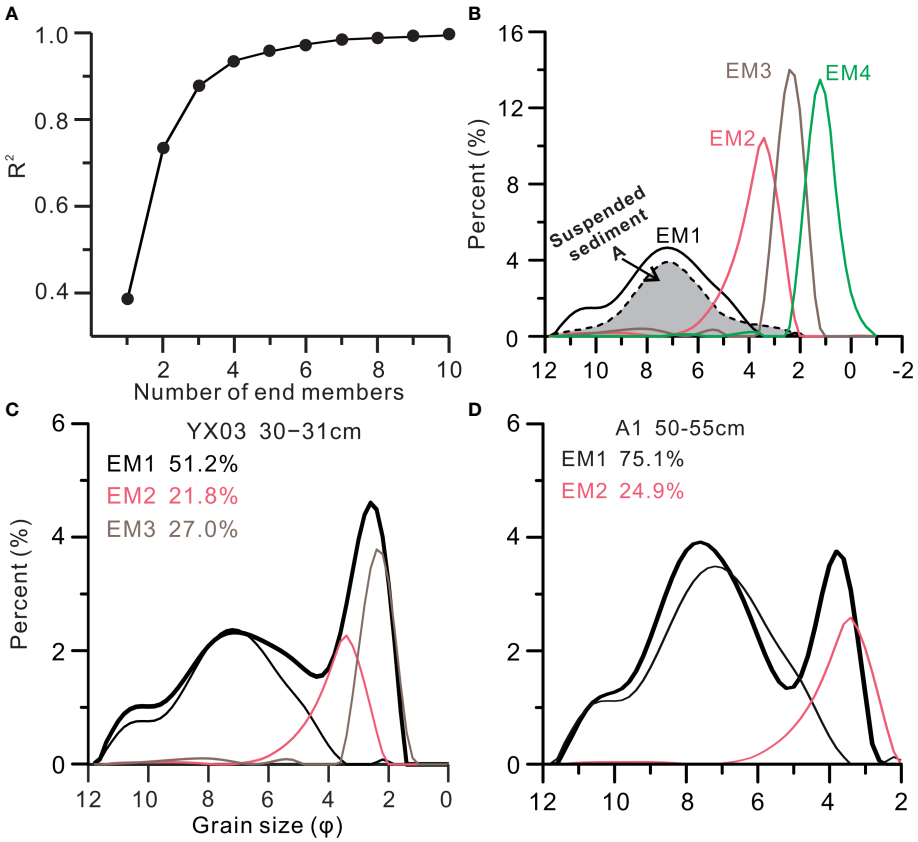

FIGURE 2
Correlation plots between the correlation coefficient (R2) and number of end-member **(A)**. **(B)** grain-size distribution of four end members. EM1 and suspended sediments from modern Pearl River (Zheng et al., 2017) have similar grain-size curves. **(C, D)** representive grain size distribution of samples from cores YX03 and A1 and the results of end-member analysis.

TABLE 1 ^{14}C-AMS dates of cores YX03 and A1.

Core	Lab ID	Depth (cm)	Dating materials	^{14}C age(BP)	Calibrated age (cal BP)
YX03	Beta497641	7–8	Mixed forams	2,210 ± 30	1,958 + 62–72
	Beta495116	29–30	Mixed forams	2,490 ± 30	2,301 + 52–61
	Beta483269	60–65	Bivalve shells	2,790 ± 30	2,700 + 55–49
	Beta375097	78–85	*Tapes literatus*	6,600 ± 30	7,312 + 53–59
	Beta375098	152–160	*Meretrix* spp.	7,630 ± 30	8,289 + 58–58
	Beta483271	257–265	Bivalve shells	7,670 ± 30	8,321 + 56–60
	Beta375099	297–304	Organic sediments	27,200 ± 180	31,152 + 115–117
A1	Beta495117	0–5	Mixed forams	1,900 ± 30	1,597 + 64–65
	Beta495118	60–65	Mixed forams	3,030 ± 30	2,946 + 69–81

Table 1 lists AMS^{14}C dates on mollusk and foraminiferal shells obtained from cores YX03 and A1. Organic materials from greenish lacustrine mud in core YX03 below 275 cm were dated to 39.5–31.2 ka BP, suggesting that the grayish mud accumulated during the Pleistocene at low sea levels. Basal Holocene deposits in core YX03 are estimated at 8,400 BP based on dates on bivalve mollusk shells. Six dates in the Holocene section show a large jump in ^{14}C ages from 7,300 BP at 80 cm to 2,700 BP at 60 cm. Section I of core YX03 was estimated to be between 8,300 BP and 7,300 BP. The upper section above 60 cm has a stable accumulation rate of ~70 cm/ka during the last 2,700 years. One ^{14}C date (1,960 BP) at the top suggests some younger sediments were lost during the rotary drilling (Table 1). In the core A1, the topmost was dated to be 1,600 BP and the fine-grained upper section (II) developed after 3 ka BP.

Grain size and end-member modeling results

The mean grain size of core YX03 varies from 4 φ to 6 φ, with an average of 4.8 φ. A clear change in grain-size fractions could be found at 60 cm, showing an obvious fine upward trend. In section I, the sand content is greater than 48% and the clay is lower than 10%. In section II, the sand, silt, and clay content are 39%, 51%, and 10%, respectively. Sediments in core YX03 exhibit very poor sorting and have multiple modes in grain-size distributions. Two distinct modes were present at 2.5 φ and 7.1 φ (Figure 2C). A secondary mode on the fine side at 10.5 φ is also clear in most grain-size curves. Another secondary mode at 5.2 φ could be found in some samples.

In core A1, the mean grain size is 6.7 φ on average, and the sorting coefficient is greater than 2. Silt is dominant in this core with an average content of 70%. In the upper section, the average sand content is less than 7%. In the lower section, sand increases to 18% and the clay content is around 14%. Three modes at 3.7 φ, 7.3 φ, and 10.1 φ are present in the grain-size distributions (Figure 2D). The mode at 7.3 φ is stably present in most samples. However, the mode at 3.7 φ is more prominent below 50 cm.

All grain-size data from the two cores and surface sediments is input into the nonparametric AnalySize to calculate end members. As shown in Figure 2A, the mean coefficient of determination (R^2) increases as the number of end members (n) increases. We determined four end members according to the inflection point in the R^2-n curve, which reproduced 94% of the dataset variance The first component (EM1) mainly consists of silt and clay with two modes at 7.1 φ and 10.1 φ. The other three components are sand-dominated. EM2, EM3, and EM4 have three modes at 3.3 φ, 2.3 φ, and 1.1 φ, respectively (Figure 2C).

On the north-western shelf of SCS, EM1 exists in most surface samples, and muddy sediments have a higher abundance (Figure 3A). The proportion of EM1 is over 90% in the Pearl River estuary. The very-fine sand component, EM2, has an average proportion of 17%. Offshore sediments south of the Jian River mouth have the highest content of EM2 (30%–40%) (Figure 3B). EM2 is the main component of surface sediments on the shelf west of Hailing Island. Coarse deposits surrounding the Hailan Island and the Leizhou Peninsula have the highest contents of EM3 (Figure 3C) and EM4. Relict sandy deposits on the eastern middle shelf, including the paleo-Pearl River delta, have high proportions of EM3 and EM4 (~20%).

Core YX03 consists mainly of three end-members: EM1, EM2, and EM3. The EM1 varies between 20% and 70% (an average of ~42%), with higher content in section II (Figure 4). The highest proportion of EM1 was found between 20 cm and 45 cm. Another end member, EM3, is also distinct in this core with an average proportion of ~35%. The variation in the proportion of EM3 is anti-phase with the EM1, showing a lower value in section II. Core A1 mainly includes two end members, EM1 and EM2 (Figure 5). The proportion of EM1 is highest between 5 cm and 50 cm, with a value of over 80%.

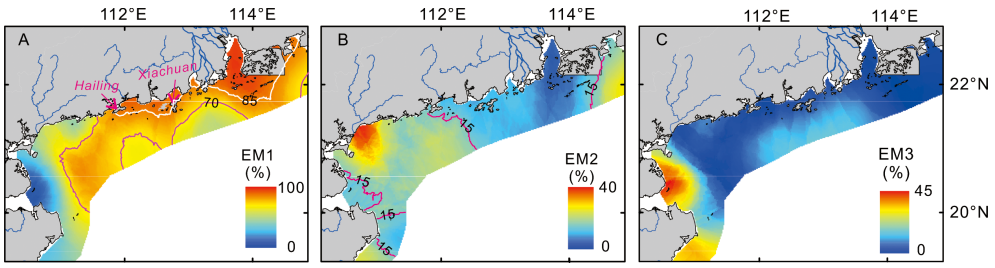

FIGURE 3
The distribution maps of three grain-size end-members (A: EM1; B: EM2; C: EM3) of surface sediments are shown on the north-western South China Sea shelf. Two solid lines in Figure 3A label the EM1 content of 85% and 70%. The purple solid lines in Figure 3B represents the EM2 content of 15%.

Geochemical compositions

From the comparison of the two elemental datasets of core YX03, the ratios of log(Zr/Al), Al/Sum, and log(K/Al) derived by the XRF core scanner have high correlations with the corresponding ratios by ICP-OES. The Zr/Al ratio and the Al content record the fining upward at 2,700 BP (Figure 4). In section I, high-resolution scanned data detect some coarse beds with a high Zr/Al ratios and low Al contents, such as at 164–181 cm, 130–135 cm, and 120–123 cm. The K/Al ratio in section I, with an average of 0.35, is higher than that in section II. The K/Al ratio is mostly less than 0.31 in section II, and it rapidly decreases at 70–55 cm. The Ti/Nb ratio in core YX03 is an average of 236 in section I, with large fluctuations. However, it shows a decreasing trend from 70 cm to the core top. The Cu/Al and Pb/Al ratios have an average of 3.6×10^{-4} and 5.4×10^{-4} and no obvious trends are found in these two ratios.

In core A1, the Zr/Al ratio and Al content correlate well with the grain-size variation. Fine sediments in section II have a higher Al content but a lower Zr concentration. The K/Al ratio

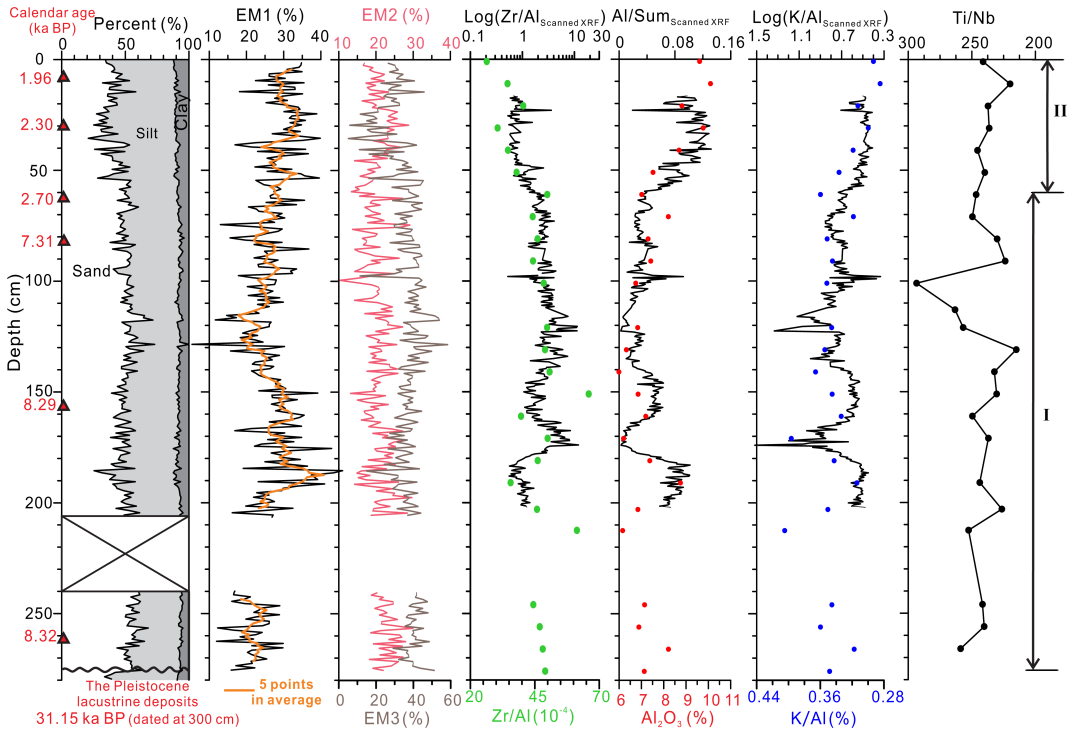

FIGURE 4
Sedimentary compositions and elemental proxies of core YX03. Elemental results of discrete samples were shown by solid dots on down-core elemental profiles collected by the XRF scanner. Red triangles on the depth scale mark ^{14}C dating samples. Sub-segments are labeled on the right side.

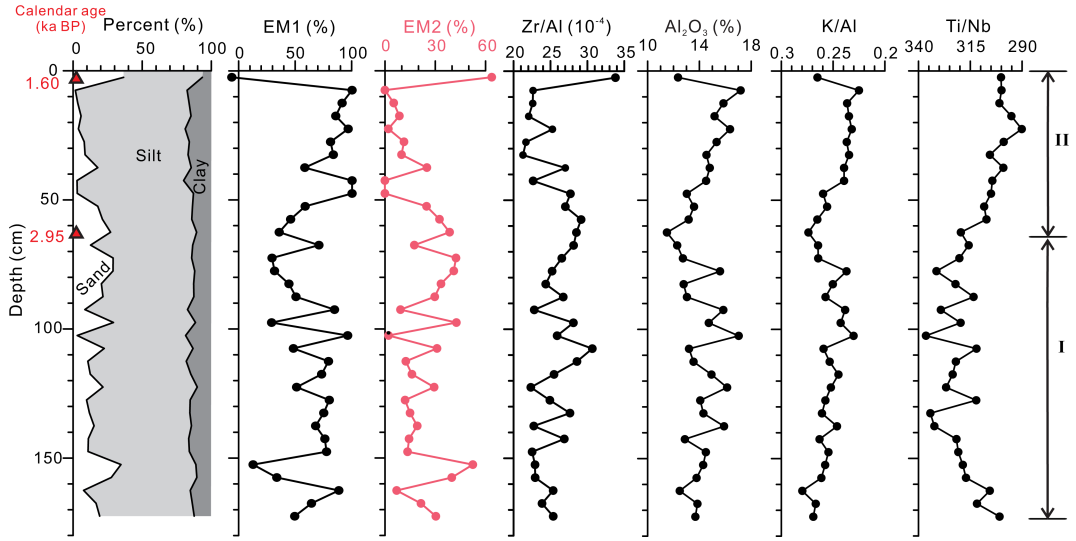

FIGURE 5
Sediment compositions and elemental proxies of core A1. Red triangles on the depth scale marked ^{14}C dates. Sub-segments were labelled on the right side.

decreased at 60 cm. The change in geochemical composition could be found in the Ti/Nb ratio, with a lower value in section II. The change in the Ti/Nb ratio was dated to 2.95 ka BP. The Cu/Al ratio shows the lowest value between 75 cm and 30 cm, and sediments above and below this segment have higher values. The highest Pb/Al ratio is present in the top 20 cm.

Discussion

Postglacial transgression and shelf sedimentation

Core YX03 on the north-western SCS shelf contains two depositional units with distinct sedimentary textures and chemical compositions. Section I was poorly sorted and sand-dominated (Figure 4). Radiocarbon dates of 8,300–7,300 BP suggest this sand bed was deposited during the middle Holocene. According to a recent report on relative sea-level changes in the northern SCS (Xiong et al., 2018), sea level rose from approximately −5 m to the present position during this period (Figure 6C). The paleo-coastline has retreated to the present shoreline since 8 ka BP, according to recent compiled paleo-geographic maps by Wei et al. (2016) and Yao et al. (2009). Combining the water depth at the coring site and sea-level positions, a paleo-water depth of 30–35 m is estimated when this transgressive sand bed accumulated between 8,300 and 7,300 years of BP. Similar transgressive sandy deposits overlying the Pleistocene terrestrial mud were also found on the middle and outer shelf of the northern SCS (Yim et al., 2006; Xiao et al., 2013; Xiong et al., 2018). These transgressive sands are inferred to be deposited in the inner and middle shelf environments (Figures 6A, B). Foraminifera analyses by Yim et al. (2006) found a high percentage of shallow-water benthonic species, such as *Ammonia beccarii* var., *Elphidium advenum*, and *A. annectens* in these transgressive sands.

Radiocarbon dates show a wide range of age inversions in transgressive sandy deposits in the south of the Pearl River Estuary, suggesting extensive reworking occurred (Yim et al., 2006; Waxi et al., 2016) (Figure 6A). In the north-western SCS, the Holocene sediments on the shelf, such as in cores YX03 and E602, mainly consist of transgressive sands (Figures 1A, 6B). Xiao et al. (2013) conducted a detailed analysis on grain size of E602 and pointed out that transgressive sands were reworked by high frequent tropical storms. The narrow range of ^{14}C dates in transgressive sands from cores YX03 and E602 suggests they were not associated with the rapid accumulation but were produced by repeated reworking. Radiocarbon dates with narrow age ranges were also reported from transgressive sands on other continental shelves (Schimanski and Stattegger, 2005; Hong et al., 2019) and some subaqueous deltas (Wang et al., 2010). The youngest dates within these transgressive sands in cores YX03 and E602 might represent the most recent disturbances by storms on the north-western SCS shelf. Radiocarbon dates from transgressive sands in core E602 on the outer shelf are older than those in cores YX03 and YJ on the inner and middle shelf (Figure 6B). The decrease in the ages of transgressive sands records the landward migration of storm-reworking zones during the Holocene. With the sea level rising, the influence of storms decreased in deep waters and mud

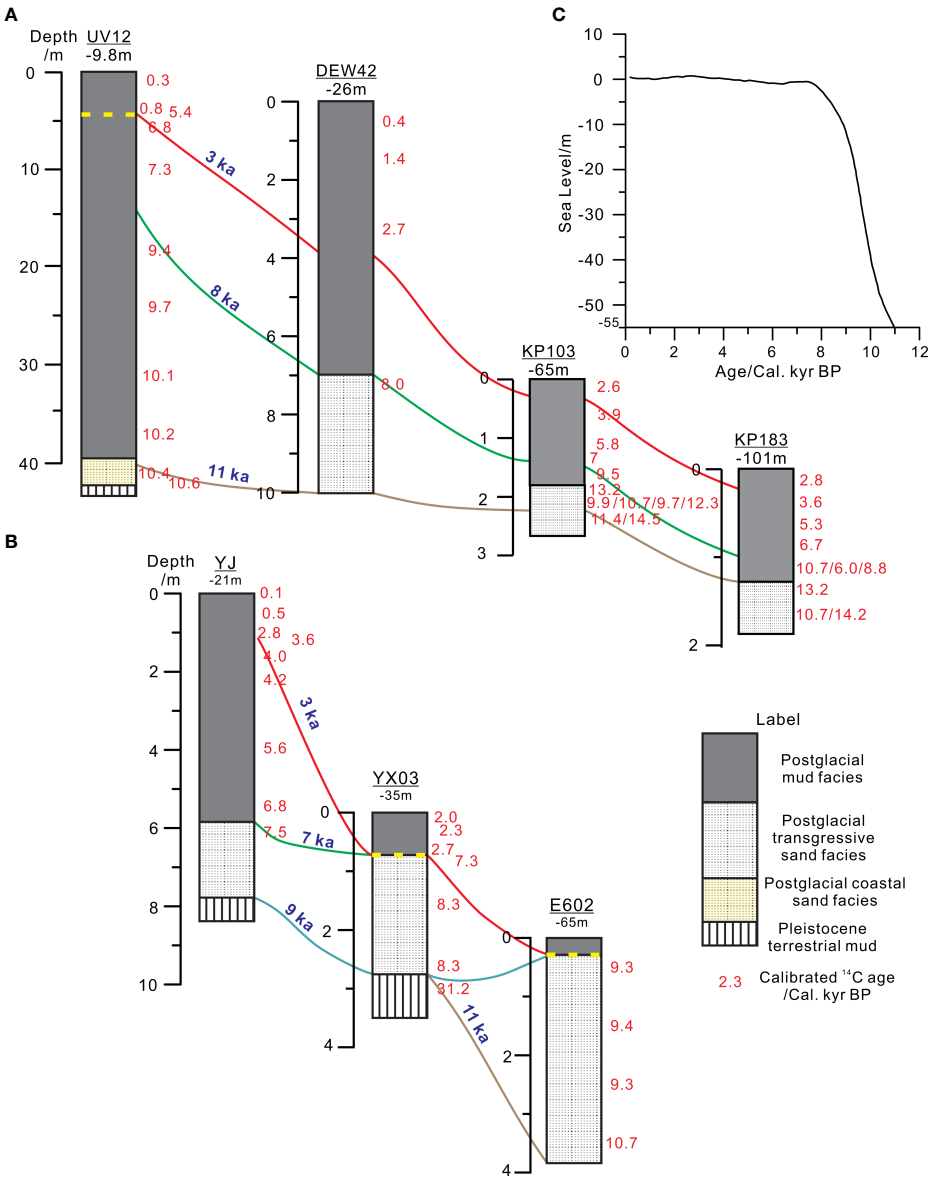

FIGURE 6
Two cross sections of Holocene sedimentary sequence on the north-western SCS shelf (**(A)** in the east; **(B)** in the west). **(C)** Sea-level changes since 11 ka BP according to Xiong et al. (2018). Reference cores were published by Xiao et al. (2013); Huang et al. (2018); Xiong et al. (2018) and Yim et al. (2006). The location of cores can be found in Figure 1A.

sediments subsequently accumulated. In the northern SCS, massive transgressive sands are directly exposed on the present seafloor. Mud sediments were only found in the subaqueous delta of the Pearl River (Yim et al., 2006; Ge et al., 2014) and in shallow waters along the western Guangdong coast (Liu et al., 2009; Xiong et al., 2018). Mud zones on the northwestern SCS shelf mostly have a thickness of less than 1 m (Figure 6B). Even in the uppermost mud deposits, the two coarse end members have high proportions. It indicates that high waves during the most energetic storms can remobilize the underlying transgressive sands and mix them with fine-grained sediments.

In summary, the Holocene sedimentation rates are low in most areas of the northwest SCS shelf, less than 30 cm/ka in most areas except 1–3 m/ka in some shallow waters. The high sedimentation rate along the western Guangdong coast is associated with the influence of the Pearl River. High proportions of transgressive deposits in the Holocene strata reflect the sediment starvation on this shelf due to rising sea

levels. With the rising sea level on a low gradient shelf, sediment supply was vastly reduced due to the increasing distance to river mouths. Under these conditions, marine processes, such as storms and tide currents, heavily reworked and homogenized the Holocene deposits. This is reflected by inconsistent ^{14}C dates in Holocene deposits. Origin studies on surface sediments in the same area also highlighted that recycled sediments accounted for a great proportion (Li et al., 2015; Li et al., 2016). Most Holocene sediments on the northern SCS shelf are intensive reworked sediments or palimpsest sediments, according to Swift et al. (1971).

Expansion of muddy zones on the shelf

On the continental shelf of the north-western SCS, the coast-attached muddy belt has a vast area of 8,000 km^2. Using shallow seismic profiles, Liu et al. (2009) and Ge et al. (2014) developed the first isopach map of the Holocene sediments on the northwest SCS shelf. According to seismic stratigraphy, this muddy wedge along the western Guangdong coast (Figure 1A) ends at around Hailing Island, and the Holocene thickness is estimated to be more than 10 m. Huang et al. (2018) retrieved a long core on the distal muddy wedge offshore Hailing Island (YJ at 21 m), and the Holocene stratum is 7.8 m thick (Figure 6B). According to stratigraphic records of core YX03 in this study and other cores reported by Yim et al. (2006), the Holocene deposits on this shelf are less than 5 m thick (mostly less than 3 m) in waters deeper than 30 m (Figures 6A,B). Moreover, the Holocene deposits only contain a very thin muddy carpet, as recorded by core YX03 (Figure 4) and other cores reported by Gao et al. (2015) and Liu et al. (2014).

The grain-size component of EM1 has a similar distribution curve to suspension sediments of the Pearl River, suggesting that EM1 represents fine-grained sediments from this large river (Figure 2B). A previous geochemical study on surface sediments on the northwest SCS shelf found that the Ti/Nb ratio was independent of the sorting process and the grain-size effect (Li et al., 2016). Bulk fluvial sediments from the Pearl River are characterized by a lower Ti/Nb ratio because of a large number of weathered sediments from granitic rocks. In core A1 near the coast, the increase in the relative proportion of EM1 at 60 cm is accompanied by a decrease in the Ti/Nb value, indicating that the fining of sediments is contributed by the Pearl River. In the nearby core YJ, muddy sediments above 5.8 m were mostly projected into the zone of the Pearl River source on a La-Th-Sc ternary diagram (Huang, 2018). Although the EM1 in the core YX03 is not as dominant as in the two coastal cores, the increase in this end member and subtle decrease in Ti/Nb ratio could also be observed in upper mud sediments (Figure 4). According to geochemical evidence, the muddy deposition on the north-western shelf of SCS is closely related to fine-grained sediments from the Pearl River.

However, chronological records show a difference in the evolution history of mud deposits on the middle shelf and in shallow waters in the north-western SCS. Radiocarbon ages from core YJ (Huang et al., 2018) indicated the muddy wedge occurred in offshore waters much earlier than other muddy deposits on the middle shelf (Figure 6B). The base of muddy deposits in YJ was dated at around 7 ka BP (Huang et al., 2018). On the middle shelf, the accumulation of mud sediments started later than 3 ka BP according to this study. Moreover, a hiatus of more than 4,000 years between shelf muddy deposits and transgressive sands in core YX03 was also observed in core E602 in the west (Xiao et al., 2013; Figure 1). Mud sediment (site Z01, which is about 10 km away from the E602 (Figure 1A)) was dated younger than 350 years using the ^{210}Pb method (Liu et al., 2014), but transgressive sands were dated older than 9,300 BP by ^{14}C ages (Xiao et al., 2013).

The review by Hanebuth et al. (2015) summarized three main initiation phases in the evolution of mud depocenters from different shelf settings at around 14 ka, 9.5–6.5 ka, and 2 ka. From previous records on the northern SCS shelf, mud belts on the outer shelf south of the Pearl River were initiated at around 10 ka BP during the transgression (Yim et al., 2006; Figure 6A). The YJ record in offshore waters along the western Guangdong Province indicates the coastal mud wedge formed after 7ka BP when modern current systems were established (Huang et al., 2018; Figure 6B). The reconstructed salinity using diatoms suggests that freshwater plumes out of the Pearl River mouth have been present since 7ka BP (Zong et al., 2006; Zong et al., 2012). A process-oriented experimental study indicated that freshwater discharge is one of the important factors inducing the formation of westward coastal currents in northern SCS (Ding et al., 2017).

However, most of the mud deposits on the middle shelf did not appear in the north-western SCS until 3 ka BP. The expansion of mud deposition from offshore waters to the middle and outer shelf has been suggested to be associated with the evolution of the Pearl River delta (Gao et al., 2015). According to Wei et al. (2016), the widespread marine inundation produced a large embayment at the mouth of the paleo-Pearl River when the sea-level rose to the present height at around 7 ka BP. Most of the fluvial sediments from the Pearl River were trapped within the paleo-estuary between 7 ka and 2 ka BP (Zong et al., 2009; Wei et al., 2016). Stratigraphic hiatuses found in the deltaic area were commonly dated between ca. 7 ka and 3 ka BP (e.g., Wei et al., 2016; Xiong et al., 2018; Chen et al., 2019) (Figures 7A, B). The hiatus found in cores YX03 and E602 on the western continental shelf is chronologically correlated with those in the Pearl River delta (Figure 7C). They reflect the sediment starvation prevailing in the outer plaeo-Pearl River estuary and on the middle shelf during this period. However, the sedimentation rate in core YJ in western offshore waters shows a significant increase during 7–3 ka BP (Figure 7D). The geochemical compositions of mud deposits in this core point

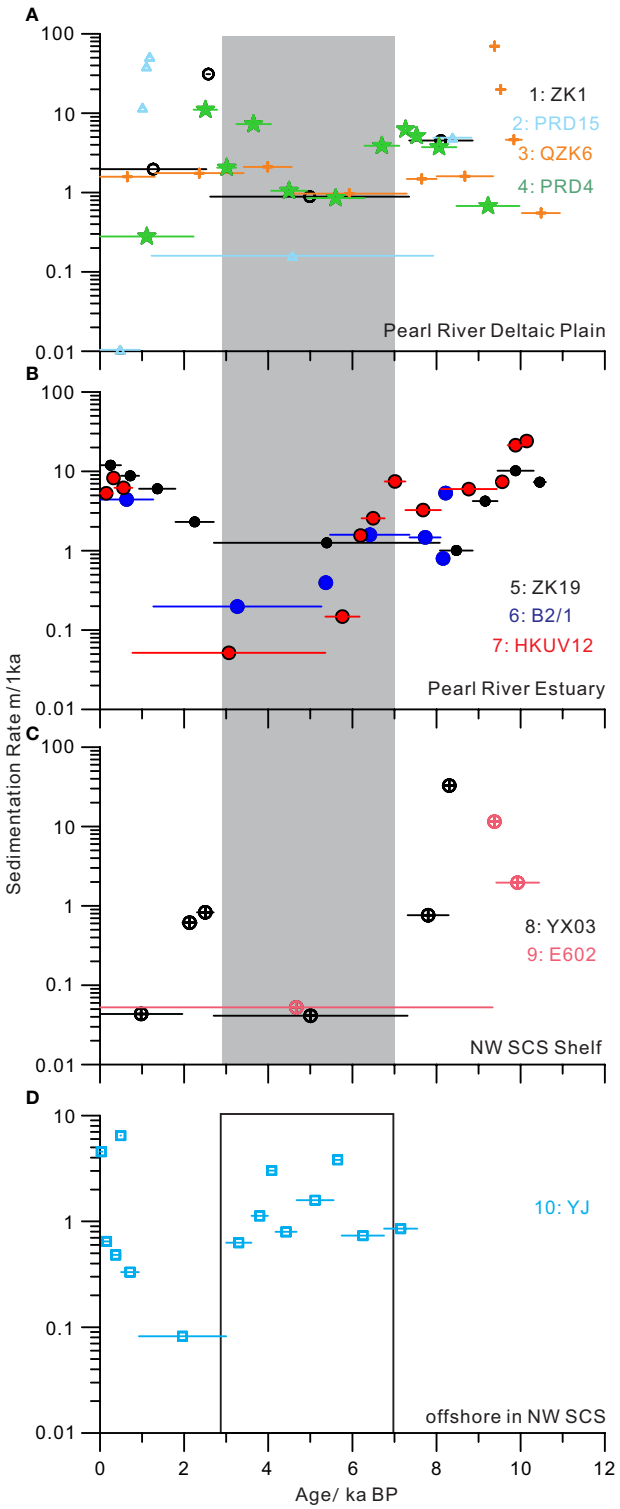

FIGURE 7
Sedimentation rates of marine deposits on the north-western SCS shelf during the past 12 ka BP. See Figure 1A for the locations of cores. Note that between ~3 and 7 ka BP the accumulation rates were low at the Pearl River delta and on the middle-and-outer SCS shelf. The low sedimentation rate during this period was not found in offshore waters. Reference cores were published by Yim et al. (2006); Hu et al. (2013); Xiao et al. (2013); Wei et al. (2016); Huang et al. (2018); Xiong et al. (2018); Chen et al. (2019) and Zong et al. (2012).

to the source of the Pearl River during this period (Huang, 2018). Widespread hiatuses in the outer estuary of the Pearl River and on the northwest SCS shelf denied a large amount of fine-grained sediment directly supplied by this big river during 7–3 cal ka BP. However, a large paleo-delta of the Pearl River was found in water depths of 30–60 m on the northern SCS shelf (Bao, 1995) (Figure 1A). This paleo-delta with an area of 4,000 km^2 was heavily reworked and relict coarse sands and gravels lay on the present sea floor (Zhong et al., 2017). Fine-grained sediments reworked from this paleo-delta might have fed the inner-shelf sedimentation through the westward coastal currents during 7–3 ka BP.

After 3 ka BP, the increased sediment discharge of the Pearl River promoted the rapid progradation of its delta (Zong et al., 2009; Wei et al., 2016). Wei et al. (2016) estimated that sediment fluxes in the Pearl River have accelerated to 50 million tons a^{-1} since 2 ka BP, from less than 30 million tons a^{-1} before. The increase in sediment flux in recent millennia was widely thought to be related to human activities (e.g., Zong et al., 2009; Wei et al., 2016) because plenty of evidence, such as diatom, pollen, estuarine $\delta^{13}C$ and stalagmite $\delta^{18}O$ indicated a weakened summer monsoon in South China (Cheng et al., 2018; Dykoski et al., 2005; Yu et al., 2011) (Figure 8A). According to the comparison of charcoal fluxes with previous peak interglacial periods in northern SCS, Cheng et al. (2018) concluded that human activities through land-use modifications completely altered the natural vegetation trend after 5–6 ka BP during the Holocene. Pollen studies widely found the rising concentration of fern spores and Poaceae in deltaic and lacustrine deposits in South China after 4–2 ka BP, suggesting human-induced deforestation and intensified agricultural activity (Zheng and Li, 2000; Wang et al., 2007; Zhao et al., 2009). In addition, significant enrichment of heavy metals in shelf sediments is also thought to be mainly associated with the intensified human

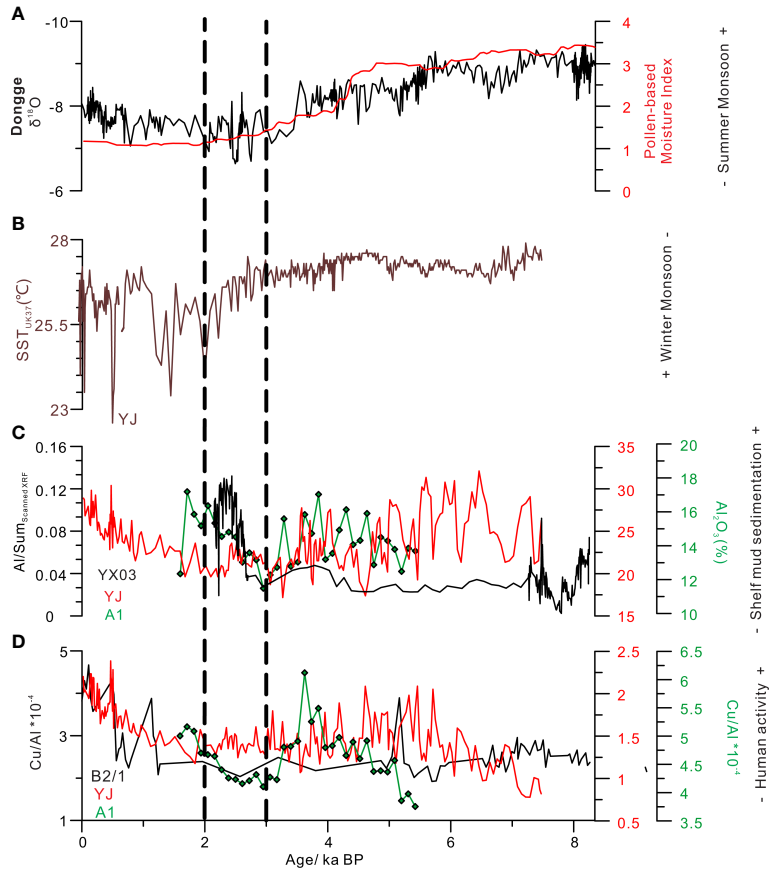

FIGURE 8
Comparison between proxy data of East Asian monsoon, shelf mud sedimentation, and human activities in the northern South China Sea in the past 8ka BP. **(A)** stalagmite $\delta^{18}O$ record from Dongge Cave (Dykoski et al., 2005); moisture index based on pollen (Zhao et al., 2009); **(B)** the strength of winter monsoon recorded by alkenone sea surface temperature of core YJ in the northwest SCS Zhang et al. (2019). **(C)** Al concentrations from cores YX03, YJ (Huang et al., 2008) and A1, recording the initiation of shelf muddy sedimentation; **(D)** The Cu/Al ratio in the Pearl River estuary (Hu et al., 2013) and on the western SCS shelf (Huang et al., 2018 and this study), showing the enhanced anthropologic activities in recent 2000 years.

activities around the northern SCS. Xu et al. (2017) recorded obvious increases in Cu, Cd, and Pb after 4 ka BP in two cores southeast of Hainan Island. The abundance of heavy metals in sediments, such as Cu and Pb, was observed to substantially increase in the Pearl River delta (Hu et al., 2013) and in cores YJ (Huang et al., 2018) and A1 (this study) near the western Guangdong coast, reflecting the expansion of mining and metal-working activities after 2 ka BP (Figure 8D). These enhanced agricultural and mining activities caused soil erosion and increased sediment fluxes of the Pearl River to a certain degree. In addition, land reclamation and dyke construction on the deltaic plain accelerated the shoreline advance of the Pearl River delta (Zong et al., 2009) and promoted sediment delivery to the shelf (Figure 9). Although there are some differences in chronology between different records around the studied area, the predominance of human activities has been significant in recent millennia. The increased fine-grained sediments escaping from the pleo-Pearl River estuary might have initiated the wide mud deposition on the western SCS shelf. Moreover, the enhanced winter monsoon after 3 ka BP might also strengthen the westward Guangdong Coastal Current and promote the transport of fine-grained sediments to the western SCS shelf. The enhanced winter monsoon has caused a significant decrease in the sea surface temperature of coastal waters in the northern SCS (Zhang et al., 2019).

As summarized by Hanebuth et al. (2015), shelf mud deposition mostly took place during the middle Holocene sea-level highstand when fine sediments were available, such as from some big rivers. Distal fine sediments from the Yellow River were transported out of Bohai and built thick muddy clinoforms south of the Shandong Peninsula during 9.5–6.5 ka BP (Liu et al., 2009). The Zhe-Min mud belt on the inner shelf of East China Sea initiated as early as 11 ka BP but rapidly aggraded after 8–7 ka BP when large amounts of fine-grained sediments escaped out of the Yangtze River delta (Liu et al., 2007; Xu et al., 2012; Li et al., 2014). In the eastern Yellow Sea, mud patches were present in the southwest of Cheju Island after 7.4 ka BP due to massive sediment supply by the Yangtze and Yellow rivers (Yoo et al., 2002). Compared with these mud depocenters, fine-grained sediments escaping out of the Pearl River estuary were limited before 3 ka BP, so only small mud patches were present in offshore waters along the western Guangdong coast (Figure 9). The expansion of mud zones occurred after 3 ka BP on the shelf of the northwest SCS. Similarly, the high accumulation rate of the mud wedge after 2 ka BP was found on the inner shelf of the East China Sea (Xu et al., 2012). Hanebuth et al. (2015) pointed out that the expansion and accelerated sedimentation of mud depocenters occurred worldwide after 2 ka BP. Although natural processes, such as coastal current systems (Xu et al., 2012) and winter monsoon (this study), were suggested playing the role in the expansion of mud depocenters on the continental shelf, human activities, including vegetation destruction and deltaic reclamation, have been agreed on the significant influence on marine mud sedimentation (Lesueur et al., 1996; Huang et al., 2018).

Conclusion

Mud deposits occupy a vast area of 8,000 km^2 on the north-western shelf of the South China Sea and consist of muddy wedges in shallow waters and wide-spread muddy belts on the

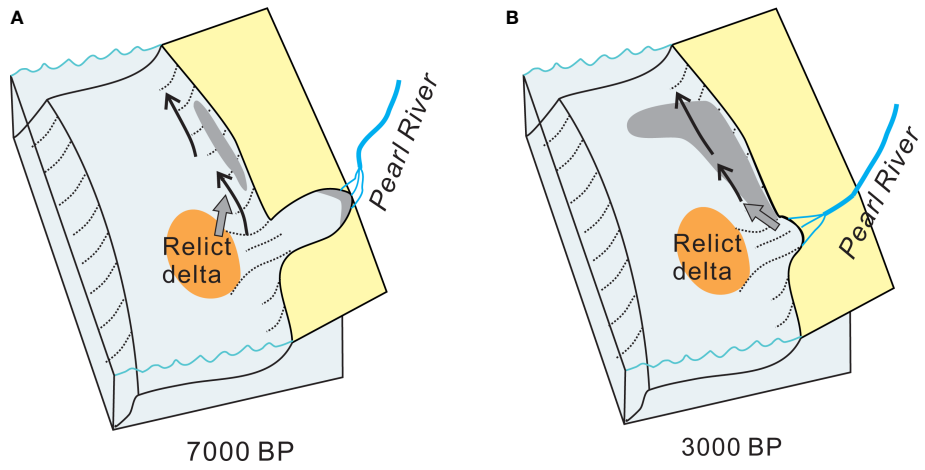

FIGURE 9
Schematic diagrams show the configurations of shelf muddy sedimentation in north-western South China Sea. **(A)** small muddy wedges have been present in shallow waters since 7 ka BP which were fed by reworked sediments from the relict delta of Pearl River. **(B)** wide-spread muddy zones on the middle shelf initiated after 3 ka BP when the paleo-embayment has been filled.

middle shelf. The Holocene evolution of this mud depositional system was reconstructed by combing sedimentary records from cores in shallow waters (Huang et al., 2018) and on the middle shelf. Mud depositional systems in the north-western SCS developed above postglacial transgressive sands which were intensively reworked by frequent storms. Mud wedges in shallow waters along the western coast, which have a thickness of more than 5 m, have formed since 7 ka BP when the sea-level rose to the present position. However, wide-spread mud belts on the shelf initiated after 3 ka BP and thin mud deposits were accumulated with a thickness of less than 1 m. The expansion of mud deposits in the western SCS shelf was associated with the evolution of the Pearl River delta and the enhanced winter monsoon. The enhanced sediment flux of the Pearl River and the acceleration of deltaic progradation caused more delivery of fine-grained sediments to the shelf after 3 ka BP. Enhanced human activities overwhelmed the monsoon in their influence on the evolution of mud deposition on the north-western SCS shelf in recent millennia.

Data availability statement

The raw data supporting the conclusions of this article will be made available by the authors, without undue reservation.

Author contributions

GL and WY conceptualized the study. LM carried out elemental analyses of discrete samples from core A1 and GL finished other analyses, including core scanning and grain-size measurements. GL prepared the original draft of the manuscript with contributions from LM and WY. All authors listed have made a substantial, direct, and intellectual contribution to the work and approved it for publication.

Funding

The study was supported by the Key Special Project for Introduced Talents Team of Southern Marine Science and Engineering, Guangdong Laboratory (Guangzhou) (GML2019ZD0206), the National Natural Science Foundation of China (42176079 and 41976062), the National Key R&D Program of China (2021YFC3100600) and the Youth Innovation Promotion Association of the Chinese Academy of Sciences.

Conflict of interest

The authors declare that the research was conducted in the absence of any commercial or financial relationships that could be construed as a potential conflict of interest.

Publisher's note

All claims expressed in this article are solely those of the authors and do not necessarily represent those of their affiliated organizations, or those of the publisher, the editors and the reviewers. Any product that may be evaluated in this article, or claim that may be made by its manufacturer, is not guaranteed or endorsed by the publisher.

References

Bao, C. W. (1995). Paleo-valleys and paleo-deltas on the continental shelf south of the pearl river (in Chinese with English abstract). *Mari. Geol. Quat. Geol.* 15 (2), 25–36

Bao, X. W., Hou, Y.J., Chen, C. S., Chen, F., and Shi, M.C. (2005). Analysis of characteristics and mechanism of current system on the west coast of Guangdong of China in summer. *Acta Oceanol. Sin.* 24 (4), 1–9.

Bassetti, M.-A., Berné, S., Sicre, M.-A., Dennielou, B., Alonso, Y., Buscail, R., et al. (2016). Holocene Hydrological changes in the rhône river (NW Mediterranean) as recorded in the marine mud belt. *Clim. Past.* 12 (7), 1539–1553. doi: 10.5194/cp-12-1539-2016

Chen, J., Ma, J., Xu, K., Liu, Y., Cao, W., Wei, T., et al (2017). Provenance discrimination of the clay sediment in the western Taiwan strait and its implication for coastal current variability during the late-Holocene. *Holocene* 27 (1), 110–21. doi: 10.1177/0959683616652706

Chen, H., Wang, J., Khan, N. S., Waxi, L., Wu, J., Zhai, Y., et al. (2019). Early and late Holocene paleoenvironmental reconstruction of the pearl river estuary, south China Sea using foraminiferal assemblages and stable carbon isotopes. *Estuar. Coast. Shelf. S.* 222, 112–125. doi: 10.1016/j.ecss.2019.04.002

Cheng, Z., Weng, C., Steinke, S., and Mohtadi, M.. (2018). Anthropogenic modification of vegetated landscapes in southern China from 6,000 years ago. *Nat. Geosci.* 11 (12), 939–943. doi: 10.1038/s41561-018-0250-1

Ding, Y., Bao, X., Yao, Z., Zhang, C., Wan, K., Bao, M., et al. (2017). A modeling study of the characteristics and mechanism of the westward coastal current during summer in the northwestern south China Sea. *Ocean. Sci. J.* 52 (1), 11–30. doi: 10.1007/s12601-017-0011-x

Dykoski, C. A., Edwards, R. L., Cheng, H., Yuan, D., Cai, Y., Zhang, M., et al. (2005). A high-resolution, absolute-dated Holocene and deglacial Asian monsoon record from dongge cave, China. *Earth. Planet. Sci. Lett.* 233 (1), 71–86. doi: 10.1016/j.epsl.2005.01.036

Gao, S., and Collins, M. B. (2014). Holocene Sedimentary systems on continental shelves. *Mar. Geol.* 352, 268–294. doi: 10.1016/j.margeo.2014.03.021

Gao, S., Liu, Y., Yang, Y., Liu, P. J., Zhang, Y., and Wang, Y. P. (2015). Evolution status of the distal mud deposit associated with the pearl river, northern south China Sea continental shelf. *J. Asian Earth Sci.* 114, 562–573. doi: 10.1016/j.jseaes.2015.07.024

Ge, Q., Liu, J. P., Xue, Z., and Chu, F. (2014). Dispersal of the zhujiang river (Pearl river) derived sediment in the Holocene. *Acta Oceanol. Sin.* 33 (8), 1–9. doi: 10.1007/s13131-014-0407-8

Hanebuth, T. J. J., Lantzsch, H., and Nizou, J. (2015). Mud depocenters on continental shelves–appearance, initiation times, and growth dynamics. *Geo-Mar. Lett.* 35 (6), 487–503. doi: 10.1007/s00367-015-0422-6

Hong, S.-H., Chang, T. S., Lee, G.-S., Kim, J. C., Choi, J., and Yoo, D.-G. (2019). Late pleistocene-Holocene sedimentary facies and evolution of the jeju strait shelf, southwest Korea. *Quat. Int.* 519, 156–169. doi: 10.1016/j.quaint.2019.04.014

Huang, C. (2018). *Holocene Climate change and human activity from an archive of continental shelf sediments in the northern south China Sea (in Chinese with English abstract)* (Doctor of Philosophy), University of Chinese Academy of Sciences, Guangzhou, CN, Guangzhou Institute of Geochemistry).

Huang, C., Zeng, T., Ye, F., Xie, L., Wang, Z., Wei, G., et al. (2018). Natural and anthropogenic impacts on environmental changes over the past 7500 years based on the multi-proxy study of shelf sediments in the northern south China Sea. *Quat. Sci. Rev.* 197, 35–48. doi: 10.1016/j.quascirev.2018.08.005

Hu, D., Clift, P. D., Böning, P., Hannigan, R., Hillier, S., Blusztajn, J., et al. (2013). Holocene Evolution in weathering and erosion patterns in the pearl river delta. *Geochem. Geophy. Geosy.* 14 (7), 2349–2368. doi: 10.1002/ggge.20166

Hu, J., Kawamura, H., Hong, H., and Qi, Y.. (2000). A Review on the Currents in the South China Sea: Seasonal Circulation, South China Sea Warm Current and Kuroshio Intrusion. *J. Oceanogr* 56, 607–624. doi: 10.1023/A:1011117531252

Lesueur, P., Tastet, J. P., and Marambat, L. (1996). Shelf mud fields formation within historical times: examples from offshore the gironde estuary. France. *Cont. Shelf. Res.* 16 (14), 1849–1870. doi: 10.1016/0278-4343(96)00013-1

Li, G., Li, P., Liu, Y., Qiao, L., Ma, Y., Xu, J., et al. (2014). Sedimentary system response to the global sea level change in the East China seas since the last glacial maximum. *Earth-Sci. Rev.* 139, 390–405. doi: 10.1016/j.earscirev.2014.09.007

Li, G., Yan, W., and Zhong, L. (2016). Element geochemistry of offshore sediments in the northwestern south China Sea and the dispersal of pearl river sediments. *Prog. Oceanogr.* 141, 17–29. doi: 10.1016/j.pocean.2015.11.005

Li, G., Yan, W., Zhong, L., Xia, Z., and Wang, S. (2015). Provenance of heavy mineral deposits on the northwestern shelf of the south China Sea, evidence from single-mineral chemistry. *Mar. Geol.* 363, 112–124. doi: 10.1016/j.margeo.2015.01.015

Liu, Y., Gao, S., Wang, Y. P., Yang, Y., Long, J., Zhang, Y., et al. (2014). Distal mud deposits associated with the pearl river over the northwestern continental shelf of the south China Sea. *Mari. Geol.* 347, 43–57. doi: 10.1016/j.margeo.2013.10.012

Liu, J. P., Xue, Z., Ross, K., Wang, H. J., Yang, Z. S., Li, A. C., et al. (2009). Fate of sediments delivered to the sea by Asian large rivers: Long-distance transport and formation of remote alongshore clinothems. *Sediment. Rec.* 7 (4), 4–9. doi: 10.2110/sedred.2009.4.4

Liu, J. P., Xu, K. H., Li, A. C., Milliman, J. D., Velozzi, D. M., Xiao, S. B., et al. (2007). Flux and fate of Yangtze river sediment delivered to the East China Sea. *Geomorphology* 85 (3-4), 208–224. doi: 10.1016/j.geomorph.2006.03.023

Nizou, J., Hanebuth, T. J. J., Heslop, D., Schwenk, T., Palamenghi, L., Stuut, J.-B., et al. (2010). The Senegal river mud belt: A high-resolution archive of paleoclimatic change and coastal evolution. *Mari. Geol.* 278 (1), 150–164. doi: 10.1016/j.margeo.2010.10.002

Park, S.-C., Lee, H.-H., Han, H.-S., Lee, G.-H., Kim, D.-C., and Yoo, D.-G. (2000). Evolution of late quaternary mud deposits and recent sediment budget in the southeastern yellow Sea. *Mari. Geol.* 170 (3), 271–288. doi: 10.1016/S0025-3227(00)00099-2

Paterson, G. A., and Heslop, D. (2015). New methods for unmixing sediment grain size data. *Geochem. Geophy. Geosy.* 16 (12), 4494–4506. doi: 10.1002/2015gc006070

Prins, M. A., Postma, G., and Weltje, G. J. (2000). Controls on terrigenous sediment supply to the Arabian Sea during the late quaternary: the makran continental slope. *Mari. Geol.* 169 (3), 351–371. doi: 10.1016/S0025-3227(00)00087-6

Qi, L., Hu, J., and Gregoire, D. C. (2000). Determination of trace elements in granites by inductively coupled plasma mass spectrometry. *Talanta* 51 (3), 507–513. doi: 10.1016/S0039-9140(99)00318-5

Reimer, P. J., Bard, E., Bayliss, A., Beck, J. W., Blackwell, P. G., Ramsey, C. B., et al. (2013). IntCal13 and Marine13 radiocarbon age calibration curves 0–50,000 years cal BP. *Radiocarbon* 55 (4), 1869–1887. doi: 10.2458/azu_js_rc.55.16947

Schimanski, A., and Stattegger, K. (2005). Deglacial and Holocene evolution of the Vietnam shelf: stratigraphy, sediments and sea-level change. *Mari. Geol.* 214 (4), 365–387. doi: 10.1016/j.margeo.2004.11.001

Southon, J., Kashgarian, M., Fontugne, M., Metivier, B., and Yim, W. W.-S. (2002). Marine reservoir corrections for the Indian ocean and southeast Asia. *Radiocarbon* 44 (1), 167–180. doi: 10.1017/s0033822200064778

Su, J. (2004). Overview of the south China Sea circulation and its influence on the coastal physical oceanography outside the pearl river estuary. *Cont. Shelf. Res.* 24 (16), 1745–1760. doi: 10.1016/j.csr.2004.06.005

Swift, D. J. P., Stanley, D. J., and Curray, J. R. (1971). Relict sediments on continental shelves: A reconsideration. *Geol. J.* 79 (3), 322–346. doi: 10.1086/627629

Tjallingii, R., Claussen, M., Stuut, J.-B. W., Fohlmeister, J., Jahn, A., Bickert, T., et al. (2008). Coherent high- and low-latitude control of the northwest African hydrological balance. *Nat. Geosci.* 1, 670. doi: 10.1038/ngeo289

Wang, W. J. (1985). Sedimentation and sedimentary facies of the pearl river mouth (in Chinese with English abstract). *Acta Sed. Sin.* 3 (2), 129–140.

Wang, P. (1999). Response of Western pacific marginal seas to glacial cycles: paleoceanographic and sedimentological features. *Mari. Geol.* 156 (1–4), 5–39. doi: 10.1016/s0025-3227(98)00172-8

Wang, W. J. (2007). *Study on the coastal geomorphological sedimentation of the south China Sea (in Chinese with English abstract)* (Guangzhou, China: Guangdong Economy Publishing House).

Wang, S., Lü, H., Liu, J., and Negendank, J. F. W. (2007). The early Holocene optimum inferred from a high-resolution pollen record of huguangyan maar lake in southern China. *Sci. Bull.* 52 (20), 2829–2836. doi: 10.1007/s11434-007-0419-2

Wang, Z., Xu, H., Zhan, Q., Saito, Y., He, Z., Xie, J., et al. (2010). Lithological and palynological evidence of late quaternary depositional environments in the subaqueous Yangtze delta, China. *Quat. Res.* 73 (3), 550–562. doi: 10.1016/j.yqres.2009.11.001

Wang, K., Zheng, H., Tada, R., Irino, T., Zheng, Y., Saito, K., et al. (2014). Millennial-scale East Asian summer monsoon variability recorded in grain size and provenance of mud belt sediments on the inner shelf of the East China Sea during mid-to late Holocene. *Quat. Int.* 349, 79–89. doi: 10.1016/j.quaint.2014.09.014

Waxi, L., Wang, J. H., Chen, H. X., Wu, J. X., and Tao, H. (2016). Elemental records of the core ZK19 in the lindingyang bay of the pearl river estuary and the paleoenvironmental implications (in Chinese with English abstract). *Trop. Geogr.* 36 (3), 343–354.

Wei, X., Wu, C., Ni, P., and Mo, W. (2016). Holocene Delta evolution and sediment flux of the pearl river, southern China. *J. Quaternary. Sci.* 31 (5), 484–494. doi: 10.1002/jqs.2873

Xiao, S., Li, R., and Chen, M. (2013). Detecting sedimentary cycles using autocorrelation of grain size. *Sci. Rep-UK.* 3, 1653. doi: 10.1038/srep01653

Xiong, H., Zong, Y., Qian, P., Huang, G., and Fu, S. (2018). Holocene Sea-level history of the northern coast of south China Sea. *Quat. Sci. Rev.* 194, 12–26. doi: 10.1016/j.quascirev.2018.06.022

Xu, F. J., Hu, B. Q., Dou, Y. G., Song, Z. J., Liu, X. T., Yuan, S. Q., et al. (2017). Prehistoric heavy metal pollution on the continental shelf off hainan island, south China Sea: from natural to anthropogenic impacts around 4.0 kyr BP. *Holocene* 28 (3), 455–463. doi: 10.1177/0959683617729445

Xu, K., Li, A., Liu, J. P., Milliman, J. D., Yang, Z., Liu, C.-S., et al. (2012). Provenance, structure, and formation of the mud wedge along inner continental shelf of the East China Sea: A synthesis of the Yangtze dispersal system. *Mari. Geol.* 291–294, 176–191. doi: 10.1016/j.margeo.2011.06.003

Yao, Y., Harff, J., Meyer, M., and Zhan, W. (2009). Reconstruction of paleocoastlines for the northwestern south China Sea since the last glacial maximum. *Sci. China Earth Sci.* 52 (8), 1127–1136. doi: 10.1007/s11430-009-0098-8

Yim, W. W. S., Huang, G., Fontugne, M. R., Hale, R. E., Paterne, M., Pirazzoli, P. A., et al. (2006). Postglacial sea-level changes in the northern south China Sea continental shelf: Evidence for a post-8200 calendar yr BP meltwater pulse. *Quat. Int.* 145–146, 55–67. doi: 10.1016/j.quaint.2005.07.005

Yoo, D. G., Lee, C. W., Kim, S. P., Jin, J. H., Kim, J. K., and Han, H. C. (2002). Late quaternary transgressive and highstand systems tracts in the northern East China Sea mid-shelf. *Mar. Geol.* 187 (3-4), 313–328. doi: 10.1016/S0025-3227(02)00384-5

Yu, F., Zong, Y., Lloyd, J. M., Leng, M. J., Switzer, A. D., Yim, W. W. S., et al. (2011). Mid-Holocene variability of the East Asian monsoon based on bulk organic $\delta^{13}C$ and C/N records from the pearl river estuary, southern China. *Holocene* 22 (6), 705–715. doi: 10.1177/0959683611417740

Zhang, Y., Zhu, K., Huang, C., Kong, D., He, Y., Wang, H., et al. (2019). Asian Winter monsoon imprint on Holocene SST changes at the northern coast of the south China Sea. *Geophys. Res. Lett.* 46 (22), 13363–13370. doi: 10.1029/2019GL085617

Zhao, Y., Yu, Z., Chen, F., Zhang, J., and Yang, B. (2009). Vegetation response to Holocene climate change in monsoon-influenced region of China. *Earth-Sci. Rev.* 97 (1), 242–256. doi: 10.1016/j.earscirev.2009.10.007

Zheng, B. X., He, J., Yao, H. Y., and Li, J. F. (2017). Grain-size distribution of suspended load and bed sediments in modaomen estuary of pearl river during flood season and implications for sediment exchange processes (in Chinese with English abstract). *J. Sediment. Res.* 42 (2), 9–15.

Zheng, Z., and Li, Q. (2000). Vegetation, climate, and Sea level in the past 55,000 years, hanjiang delta, southeastern China. *Quat. Res.* 53 (3), 330–340. doi: 10.1006/qres.1999.2126

Zhong, Y., Chen, Z., Li, L., Liu, J., Li, G., Zheng, X., et al. (2017). Bottom water hydrodynamic provinces and transport patterns of the northern south China Sea: Evidence from grain size of the terrigenous sediments. *Cont. Shelf. Res.* 140, 11–26. doi: 10.1016/j.csr.2017.01.023

Zhou, Q. K. (2014). *Numerical research on evolution character of submarine sand waves in the northern south China Sea (in Chinese with English abstract).(Master)* , First Institute of Oceanography,State Oceanic Administration, Qingdao, CN, First Institute of Oceanography).

Zong, Y., Huang, G., Switzer, A. D., Yu, F., and Yim, W. W. S. (2009). An evolutionary model for the Holocene formation of the pearl river delta, China. *Holocene* 19 (1), 129–142. doi: 10.1177/0959683608098957

Zong, Y., Lloyd, J. M., Leng, M. J., Yim, W. W. S., and Huang, G. (2006). Reconstruction of Holocene monsoon history from the pearl river estuary, southern China, using diatoms and carbon isotope ratios. *Holocene* 16 (2), 251–263. doi: 10.1191/0959683606hl911rp

Zong, Y., Yu, F., Huang, G., Lloyd, J. M., and Yim, W. W. S. (2012). The history of water salinity in the pearl river estuary, China, during the late quaternary. *Earth Surf. Proc. Land.* 35 (10), 1221–1233. doi: 10.1002/esp.2030